Applied Nanoscience (2019) 9:93–103
https://doi.org/10.1007/s13204-018-0898-2

ORIGINAL ARTICLE

Facile synthesis of zinc oxide crystal and insight into its morphological effect on organic dye photodegradation in water

Qi Sun[1] · Jianmei Li[1] · Zhentian Yan[1] · Xiru Zhang[1] · Tao Le[1]

Received: 14 July 2018 / Accepted: 15 October 2018 / Published online: 27 October 2018

Abstract

Metal oxides particularly for zinc oxide (ZnO) particles are well-known to exhibit photocatalytic activities. However, the specific morphology and superstructure of nanomaterials can significantly influence this capacity. Here, it is shown that different crystalline structures of ZnO particles are provided by a facile one-step wet-chemical route. One possible formation mechanism has been elucidated for the fabrication of distinct metal oxide samples including flower-like, sphere-like and leaf-like ZnO under different synthesis conditions. It is also found that the photodegradative performance for organic dye is directly correlated to the morphological properties of these as-prepared catalysts; the higher the active surface area the better is the photocatalytic efficiency. Not only can ZnO structure with abundant mesoporous aggregated by leaf-shape arrays lead to more methylene blue immobilization, but also generate more photoinduced electrons and holes on the crystalline surface. The results also illustrate that the morphology-dependent catalytic performance can be further improved combining with other optimized photodegradative conditions (e.g. pH, illumination mode). The present study can lead to new metal oxide with high-performance important for photocatalytic and environmental applications.

Keywords Zinc oxide · Photocatalytic performance · Structural transformation · Morphological effect

Introduction

Undoubtedly, water pollution exacerbates in the recent past, usually resulting by human activities. As major sources of water pollution, various synthetic dyes are commonly essential to many industrial process, especially textile, plastics, leather goods and food industries (Ratna 2012; Sonderegger et al. 2015). However, unpleasant effluent is often occurred by the discharge of inadequately treated wastewater into natural bodies of water, which in turn damages public health and the natural biological communities. Accordingly, it is crucial to prevent and purify water from such organic dye contamination. Nowadays, sewage disposal can be achieved by some appropriate methods, such as coagulation or adsorption treatment (Ali 2014; Allegre et al. 2004; Nguyen et al. 2012). Nevertheless, these procedures are usually limited by failure for the transformation of hazardous pollutants into the innocuous substances, and most are energy or/and cost intensive (Hegab and Zou 2015; Zhao et al. 2015). Therefore, the development of some cost-effective and environment-friendly techniques for the degradation of these refractory and toxic chemicals in water have drawn a lot of attention in the near future. Comfortingly, photocatalytic technology has broadened the way of sewage treatment, which is characterized by low cost, satisfied energy consumption and sustainable use. As for photocatalysis with high performance, it is significant to choose suitable material for the degradation of organic pollutants.

As a well-known metal oxide, zinc oxide (ZnO) is near to an ideal candidate and has received much attention for practical applications on environmental issues in the past few years. As a vitally important semiconductor material, ZnO is characterized by a wide band gap (~3.37 eV) as well as a large exciton binding energy (60 meV) at room temperature. And a large amount of native defect sites existed in the surface of ZnO can further endow the particle with a high photosensitivity (Arfaoui et al. 2017; Hernandez et al. 2015). ZnO performs comparatively higher reaction rate and

✉ Qi Sun
sunqi2017@cqnu.edu.cn

✉ Tao Le
hnxylt@163.com

[1] College of Life Sciences, Chongqing Normal University, No.37 Chengzhong Road, Shapingba District, Chongqing 401331, People's Republic of China

can produce reactive oxygen ions more efficiently than titanium oxide (TiO_2) (Carraway et al. 1994). ZnO has emerged to be a promising alternative to TiO_2 due to its excellent optoelectronic, catalytic and photochemical activities along with its low cost (Du et al. 2013; Li et al. 2010). In addition to the advantages of multiple preparation procedures and good biocompatibility, ZnO can also be used in the acidic or alkaline conditions through the proper treatment (Assadi et al. 2012). Consequently, ZnO has been often considered to be an efficient photocatalyst agent for applications of wastewater purity and environmental restoration.

On the other hand, ZnO particles have a more diverse and complex morphological structures than TiO_2. Obviously, the specific morphologies and structures of these nanoparticles should play a significant role during the process of photocatalytic degradation. So far, a variety of strategies including physical, chemical and biological routes have been developed to fabricate ZnO particles with well-defined morphological characteristics (Ali et al. 2017; Anas et al. 2015; Chuang et al. 2017). Aggregates composed of these above mentioned basic shape nanoparticles have also been obtained. Nowadays, some scientists make effort to develop ZnO-based photocatalysts to purify industrial effluent and environmental remediation (Hong et al. 2016; Xue et al. 2015). However, the correlation between crystalline morphology and its catalytical performance has not been investigated extensively so far. There is poorly information about the morphological effect of metal oxides on organic pollutants degradation in water. Apparently, for targeted acquirement of efficient sewage disposal agent, it is essential to fully elucidate the effect of material's morphology and structure on the photocatalytic performance of metal oxide. Herein, fabrication of ZnO particles with three kinds of morphology was conducted by employing a facile one-step wet-chemical strategy. Material characterization and formation mechanism for as-prepared ZnO samples were then elucidated and the dependence of the photocatalytic efficiency on crystalline morphology and superstructure was also discussed in detail. Moreover, this study also propose how to improve the photodegradative efficiency of these ZnO catalysts.

Materials and methods

Preparation of ZnO particles

Zinc sulfate heptahydrate ($ZnSO_4{\cdot}7(H_2O)$), sodium hydroxide (NaOH), citric acid monohydrate (CA, $C_6H_8O_7{\cdot}H_2O$) and methylene blue (MB, $C_{16}H_{18}ClN_3S$) were obtained from Chengdu Chemical Reagent Co.Ltd in China. These chemical reagents were of analytical grade and implemented without further purification. In a typical wet-chemical procedure (seen Fig. 1), 35 mL of NaOH solution (4 mol/L) was added dropwise into 50 mL of zinc sulfate heptahydrate solution (1 mol/L) under vigorous stirring at 4 °C. For ZnO sample A, additional deionized water was then added to the above mentioned reaction system to obtain 100 mL of precursor. The precursor was subsequently heated to 90 °C for 2 h. For ZnO sample B, a certain volumes of CA solution and deionized water were, respectively, added to the reaction system to obtain a precursor mixture containing 0.32 mol/L CA. And the following reaction conditions were consistent with the preparation of A-ZnO sample. In addition, no CA solution is needed for the synthesis of ZnO sample C and its reaction precursor is the same as A-ZnO sample. But the difference is that the precursor was heated to 60 °C for 2 h. Finally, three nanosized ZnO samples in white color with different microstructures were obtained after filtration and vacuum drying as shown in Fig. 1.

Material characterization

The crystal properties of the prepared ZnO samples were first determined with a Rigaku D/Max-2400 X-ray diffractometer

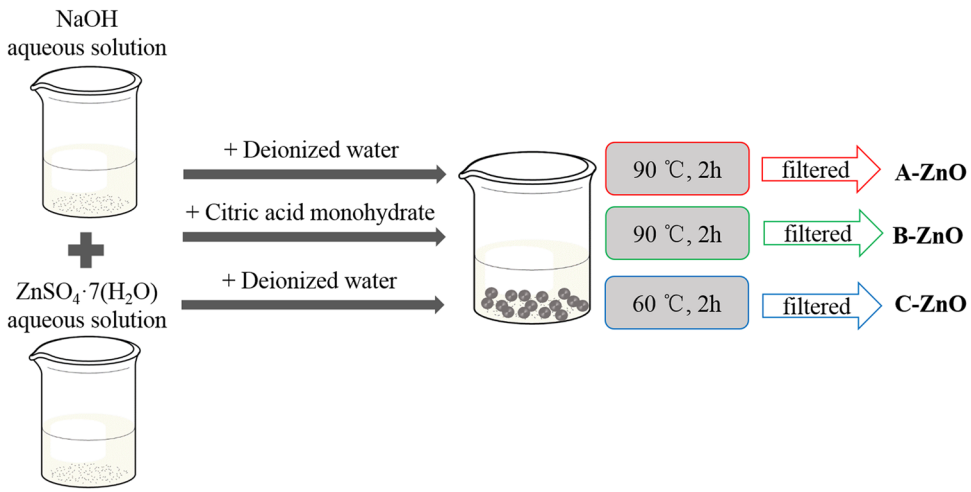

Fig. 1 Fabrication of distinct zinc oxide samples under different synthetic conditions

(XRD, Rigaku, Japan). Morphology and superstructure of ZnO particles were then evaluated by a SU-3500 scanning electron microscopy (SEM, Hitachi, Japan) and a FEI Tecnai G2-F30 transmission electron microscopy (TEM, FEI, USA). The Brunauer–Emmett–Teller gas sorptometry study was next operated by N_2 adsorption and desorption at 77 K in a model ASAP 2020 Plus HD88 specific surface and porosity analyzer (BET, Micromeritics, USA). And the Barrett–Joyner–Halenda (BJH) approach supported by the desorption branch of the N_2 isotherm was applied to evaluate the corresponding pore size distribution and total pore volume.

Detection of photocatalytic activity

To estimate the morphology-related photocatalytic activity for ZnO crystals, methylene blue (MB) was chosen as the model organic dye under different reaction conditions. All photocatalytic tests were carried out in a photocatalytic reactor system, consisting of an aqueous MB solution (10 mg/L, 80 mL) and a proper amount of the specific ZnO sample. In all photodegradation experiments, the final concentration of the obtained ZnO suspension was controlled at 0.05 wt%. The photocatalytic degradation of MB by ZnO material following the above mentioned reactor system was evaluated under multiple irradiation modes, including natural solar (600–1000 W/cm^2 real sunlight) and ultraviolet (UV) illumination (250 W mercury lamp of $\lambda_{max} = 365$ nm), respectively. Before photocatalytic evaluation, the reaction mixture containing MB solution and ZnO particles was first magnetically stirred in the dark for 30 min to achieve a complete adsorption_desorption equilibrium for both reactants. The suspension was then directly exposed to illumination and a certain volume of the reaction solution was collected at definite time intervals. Prior to UV–Vis adsorption study, the suspension was first centrifuged to separate the catalyst and the dye solution. The absorption spectrum of the MB aqueous solution was recorded with UV–Vis spectrophotometer in the range of 200–800 nm. Similarly, the blank control group was established for all photocatalytic experiments in this work. The photocatalytic efficiency (%) for catalyst-degraded organic dye was estimated in terms of alterations in absorption value of the MB aqueous solution (Das et al. 2017).

Results and discussions

Characterizations of the synthesized ZnO samples

The phase compositions of as-prepared ZnO powder were first confirmed by X-ray diffraction (XRD). As shown in Fig. 2, the diffraction peaks of all prepared metal oxide

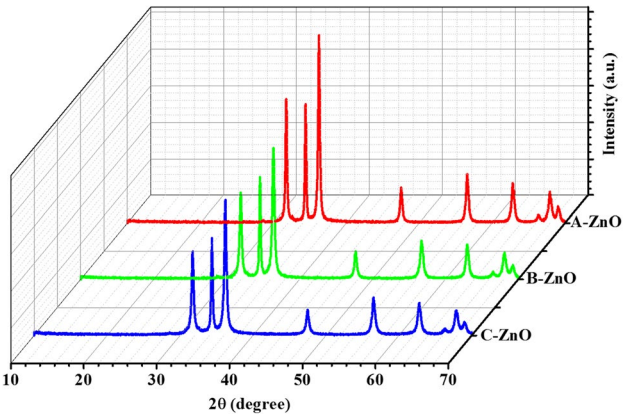

Fig. 2 X-ray diffraction patterns of as-synsthesis ZnO samples

samples are sharp and intense, proving they possess highly crystalline nature.

XRD patterns of these ZnO crystals present almost the same diffraction peaks at around 31.8°, 34.4°, 36.3°, 47.5°, 56.6°, 62.9°, 66.4°, 68.0° and 69.1°, corresponding to (100), (002), (101), (102), (110), (103), (200), (112) and (201) of the hexagonal wurtzite planes of ZnO (JCPDS card number: 36-1451), respectively (Hong et al. 2016). These results indicate that the obtained ZnO samples are all characterized by a polycrystalline hexagonal wurtzite structure. Since no other diffraction peaks were found in all patterns, it can be proved that there is no secondary phase existed in these crystalline samples. However, due to the adsorption of the reaction substrates (e.g. zinc sulfate heptahydrate or citric acid monohydrate) on the surface of particles, some certain impurities inevitably present in these ZnO powder obtained by precipitation method. On the other hand, by comparing the half-width of these crystal peaks as demonstrated in XRD results, the crystal size order of the three ZnO particles is A-ZnO > C-ZnO > B-ZnO.

The general morphologies of as-prepared diverse ZnO particles are depicted by SEM as shown in Fig. 3. For sample A, the prepared ZnO particle was characterized by well-defined flower-like appearance with approximately 3.36 μm in average particle size (Fig. 3a). From the high magnification image, it is found that A-ZnO has a branchy structure that consists of many hexagonal prisms with a tip end (Fig. 3d). With the addition of 320 mmol/L CA, ZnO particle transformed from the branchy structure to a porous microsphere with an average diameter of 2.14 μm (Fig. 3b). The magnified image of the microsphere indicated that B-ZnO has an uneven and rough surface (Fig. 3e). After the change of the preparation condition (no CA adding and reduction of reaction temperature), the irregular stacking pattern began to exist in sample C (Fig. 3c). The enlarged SEM micrographs showed that C-ZnO was composed of leaf-like superstructures (Fig. 3f).

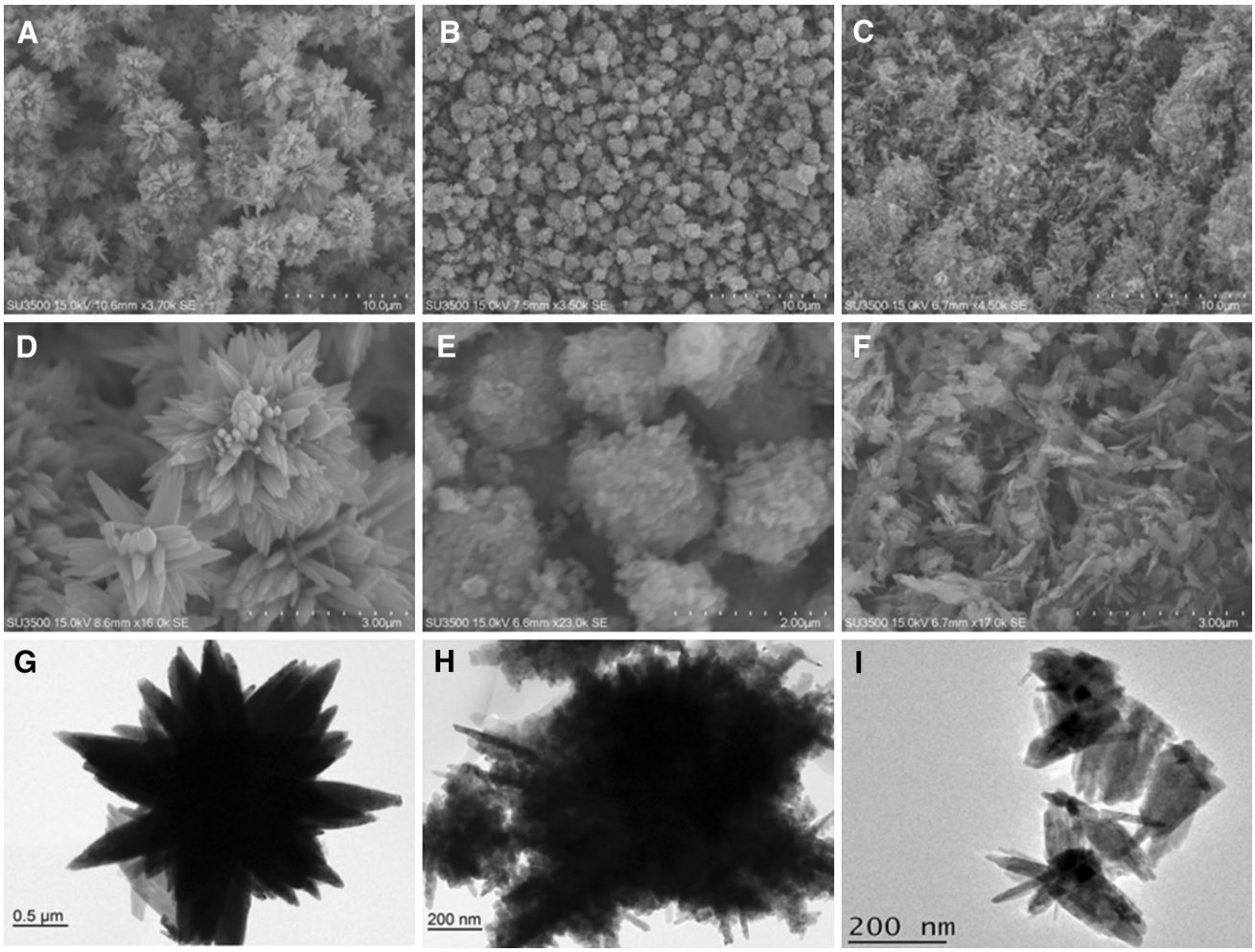

Fig. 3 SEM and TEM images of ZnO particles with different magnifications, including (**a, b, g**) flower-like A-ZnO, (**b, e, h**) sphere-like B-ZnO and (**c, f, i**) leaf-like C-ZnO

The crystallite structures of diverse ZnO particles were further determined through TEM (Fig. 3g–i). Figure 3G shows that A-ZnO product is constructed from nano-fusiform emerged from the centers to form flower-like particle and the TEM observation (Fig. 3g) was in good agreement with the SEM results (Fig. 3a, d). Figure 3h shows that the porous microsphere of B-ZnO has jagged edges with an inhomogeneous color. This TEM projection (Fig. 3h) is consistent with that of the SEM observation (Fig. 3e) wherein the porous structure is characterized by the uneven and rough surface. It is also found that the hydrothermal reaction temperature play a vital role in the morphology of the as-obtained ZnO hierarchical structures. With the decreasing the hydrothermal reaction temperature from 90 to 60 °C, a large number of flower-like structures as shown in A-ZnO disappear. Comparison of the ZnO sample images in Fig. 3 indicates that the color of TEM image (Fig. 3i) for C-ZnO particle is homogeneous and much shallower than other ZnO samples (Fig. 3g, h). By combing SEM results, the prepared C-ZnO particles should possess a typical mesoporous structure instead of a solid structure. Moreover, the HRTEM detection for C-ZnO was also shown in Fig. 4a and the interplanar spacing was estimated to be 0.26 nm, corresponding to the lattice distance of the (002) lattice plane of wurtzite ZnO (Hui et al. 2016). The Energy Dispersive X-Ray Spectroscopy (EDS) spectrum in Fig. 4b further confirmed the existence of oxygen and zinc elements in sample C, further indicating that ZnO crystal was successfully obtained. The weight percentage of two elements in C-ZnO is 70.32% for zinc and 29.68% for oxygen, respectively.

To examine the surface nature of the prepared ZnO samples, BET gas sorptometry study was next carried out in this work. Figure 5 represents the nitrogen adsorption–desorption isotherms and Barrett-Joyner-Halenda (BJH) pore size distribution plots (inset in Fig. 5) determined from the desorption branch of the N_2 isotherms for three ZnO samples. The obtained N_2 adsorption–desorption isotherms for A-ZnO (Fig. 5a) and B-ZnO (Fig. 5b) can be identified as

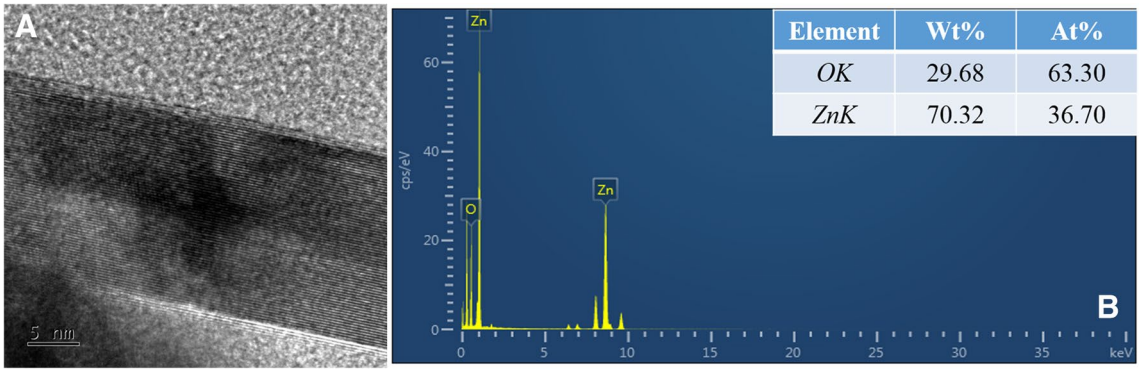

Fig. 4 High resolution transmission electron microscopy (HRTEM) detection (**a**) and energy dispersive X-Ray spectroscopy spectrum (**b**) of leaf-like ZnO sample

type II (IUPAC classification). But the adsorption amount of B-ZnO is much higher than that of sample A. In addition, the N_2 isotherm of C-ZnO basically corresponds to IUPAC type IV and has a hysteresis loop above $P/P_0 = 0.6$. Thus, the existence of mesoporous can be speculated in the leaf-like architecture by the N_2 adsorption isotherm (Miao et al. 2016; Wang et al. 2014). Moreover, the pore size distribution, obtained from desorption data and evaluated from the isotherm using the BJH model, revealed that the prepared ZnO crystals contain different pore size. BJH adsorption average pore size is 17.55 nm for C-ZnO, which is substantially larger than that of the other two crystals (13.79 nm for A-ZnO and 13.53 nm for B-ZnO, respectively). The pore-size distribution curve (inset in Fig. 5a) indicated that the small pores with characteristic peaks at 1.9 and 3.4 nm in sample A. With the adding of citric acid (320 mmol/L), the ZnO flower-like structure began to develop into a solid sphere. And the position of the peaks for B-ZnO gradually shifted to the larger pore width (inset in Fig. 5b). These mesopores are presumably originated from the spaces among the small nanocrystallites within ZnO particles (Cho et al. 2009; Wang et al. 2017). Nevertheless, the sharp distribution of mesopores around 8.7 nm was obtained from the corresponding pore size distribution curves (inset in Fig. 5c). This result could indicate that C-ZnO has high mono-dispersion and possesses a number of macropores aggregated by leaf-like superstructures. The tendency of the above observed variations is in line with the difference in the overall pore volume and surface area of as-synthesized ZnO samples. BET results show that both leaf-like C-ZnO and sphere-like B-ZnO have superior active surface areas (S_{BET}) that can be calculated as 13.86 and 13.38 m^2/g, respectively. Meanwhile, the single-point adsorption total volumes of pores at $P/P_0 = 0.9896$ are 0.0543 and 0.0623 cm^3/g for above mentioned metal oxides, respectively. In contrast, the S_{BET} and the total pore volume sharply decrease in numerical value (corresponding to 3.69 m^2/g and 0.012 cm^3/g, respectively) for flower-like A-ZnO crystal. Obviously, the extremely high surface area and large pore volume are relatively beneficial to the catalytic efficiency.

Evaluation of ZnO-photocatalytic performance

The present work performs a simple hydrothermal approach for the fabrication of ZnO particles with different hierarchical structures to evaluate their photocatalytic efficiency for the degradation of MB dye under diverse irradiation conditions at room temperature. For photocatalytic evaluation, as-prepared ZnO samples were first chosen to degrade MB dye under 250 W UV illumination in this work. The UV–visible absorption spectra of MB solution as a function of irradiation time and the rate of degradation in the process of photodegradation are demonstrated in Fig. 6. It needs to state that the difference in absorption intensity of MB solution should ascribe to normal variation in concentration due to fresh preparation of the MB solution for each sample test. And the characteristic absorbance of MB at 664 nm was chosen to evaluate the photodegradation process. Meanwhile, the alterations of MB dye color over the photocatalytic time are also shown in the insets of Fig. 6a–c. All MB dye solution in the presence of ZnO catalyst have similar experimental phenomenon but different peak changes. Three ZnO samples exhibit different performances toward organic dye photodegradation mostly resulting from the crystalline morphology and structure. In contrast, almost no degradation of blue dye was occurred in the absence of ZnO powder under 250 W UV irradiation as depicted in Fig. 6d.

Of these synthesized ZnO samples, A-ZnO may be not conducive to the improvement of the photocatalytic efficiency because the dye color hardly changes. Its degradation rate is merely 32.68% within 80 min, as shown in Fig. 7a. C-ZnO with leaf-like superstructure exhibits the best photocatalytic performance and sphere-like B-ZnO is in the second place. Under 250 W UV irradiation within

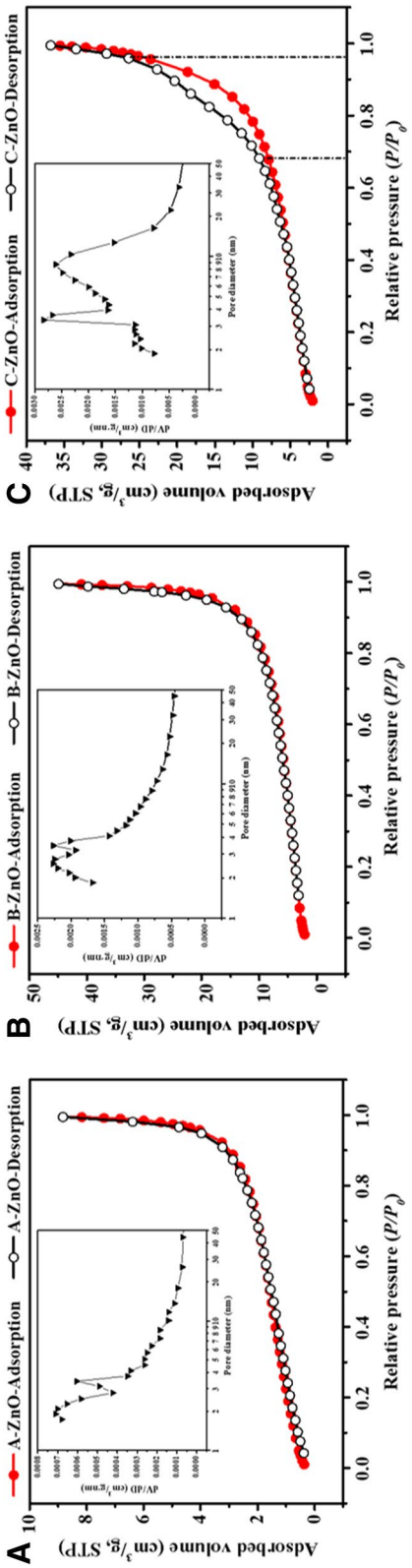

Fig. 5 Nitrogen adsorption–desorption isotherms and BJH desorption pore size distribution of different ZnO samples, including **a** flower –like A-ZnO, **b** sphere-like B-ZnO and **c** leaf-like C-ZnO, respectively

80 min, the degradation efficiency for MB was 83.51% and 54.64% for both photocatalysts, respectively. Noticeably, MB can be completely degraded within 2.5 h under catalytic action of C-ZnO powder. The differentiation of MB photodegradation is more pronounced in Fig. 7b and it shows the plots of the relative degradation (C/C_0) of dye solution versus reaction time, in which C_0 and C represent the initial level and time-dependent residual concentration of MB solution, respectively. The self-degradation of MB without the catalytic effect can be neglected as shown in blank group, demonstrating that the degradation of the color dyestuff is definitely caused by ZnO powder. The curves of ln (C_0/C) versus degradation time (Fig. 7c) are almost linear, suggesting that the photodegradation of MB dye with ZnO catalyst followed the pseudo first-order reaction kinetics ($\ln(C_0/C) = kt$). The photocatalytic efficiency of different ZnO catalysts can be further quantitatively compared via calculating reaction rate constant k values (Fig. 7c). It can estimate that k values for three ZnO samples in terms of flower, sphere and leaf-like superstructure are 0.0049, 0.010, and 0.0228 min^{-1}, respectively. Especially for leaf-like C-ZnO hierarchical microstructure, it presents a much higher kinetic constant for the MB degradation than ZnO and some other photocatalysts reported elsewhere (Das et al. 2017; Mujtaba et al. 2015; Wang et al. 2017). For example, Subhra et al. synthesized a hierarchical flower-like MnO_2 nanocomposites and its pseudo first-order rate constant was calculated to be 0.0168 min^{-1} under UV irradiation (Das et al. 2017). And the kinetic constant for the ZnO particles with a porous flower-like structure in a recent study was reported to be 0.0126 min^{-1} (Wang et al. 2017). Herein, the obtained results indicate that the stacking-lamellar structure in our study is favorable for improving the degradation efficiency of ZnO photocatalyst.

Besides, the photodegradation performance of MB for C-ZnO photocatalyst under different treatments are conducted as shown in Fig. 8. The corresponding rate constants of the degradation reactions are further assessed for UV and solar irradiation followed the pseudo-first-order kinetic model. Results (illustrated in Fig. 8a, b) indicate that C-ZnO sample possesses a significant higher photo-reaction rate constant under 250 W UV irradiation compared to the actual sunlight (0.0228 min^{-1} vs. 0.0062 min^{-1} for both k values). To ascertain the effect of the amount of ZnO catalyst used and to avoid unnecessary excess photocatalyst, a series of detections were conducted by varying the concentration of ZnO particles (0.01–0.5%, wt%). The photodegradation efficiency of MB as a function of irradiation time under 250 W UV treatment was plotted in Fig. 8C. Obviously, the increasement of the amount of photocatalyst ZnO should be beneficial to the enhancement of the active sites which consequently leads to enhanced production of reactive hydroxyl radicals

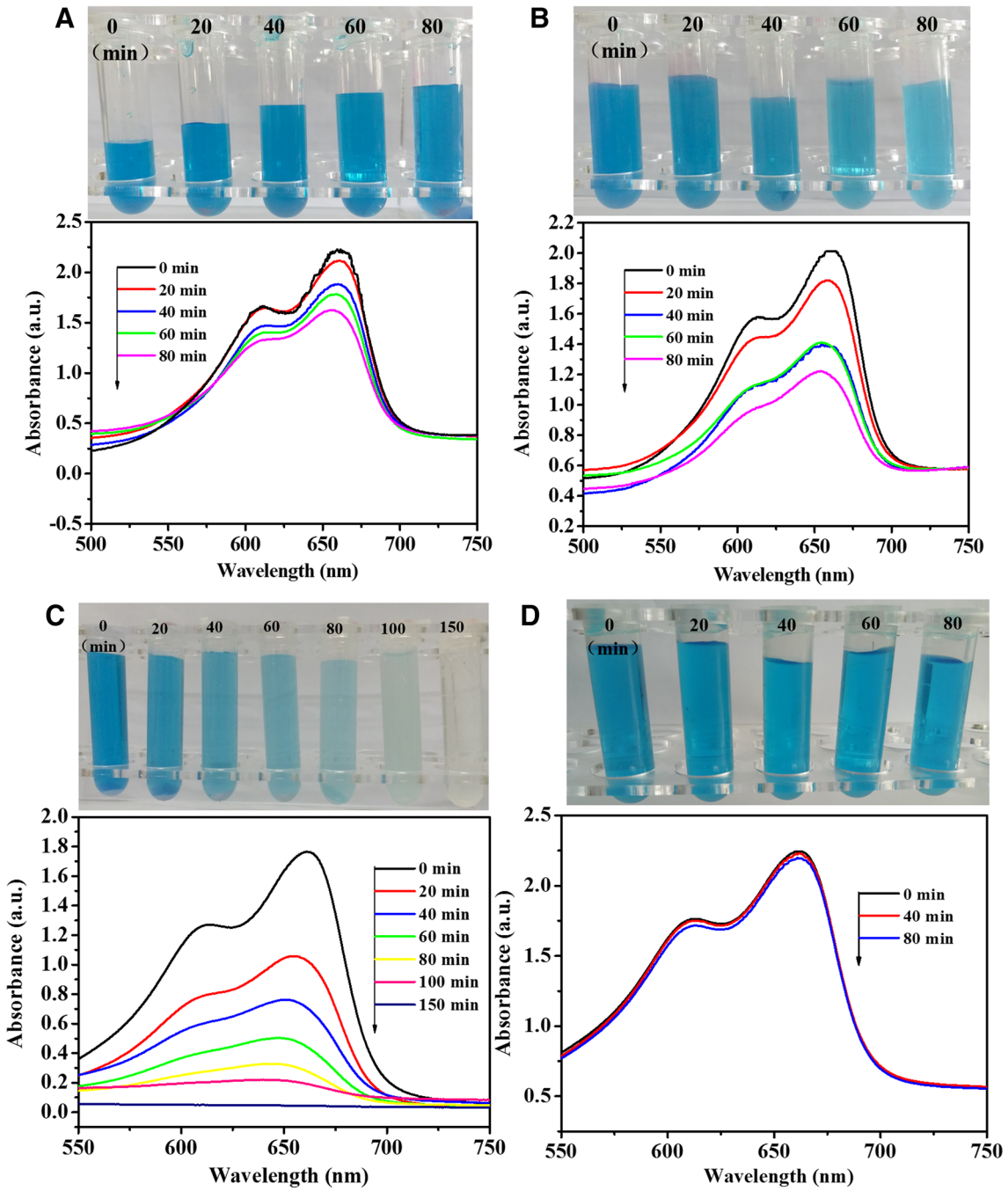

Fig. 6 UV–Vis spectra of MB solution upon photodegradation treated by distinct ZnO materials under 250 W ultraviolet irradiation, including **a** A-ZnO, **b** B-ZnO and **c** C-ZnO and **d** blank control group without the addition of ZnO particles. The above inset is the color changes of MB solution upon photodegradation under different irradiation periods

(OH·). Furthermore, the more the photocatalyst particles used, the higher number of MB molecules adsorbed, thus the faster the photocatalytic degradation proceeded (Fox and Dulay 1993). In this study, the maximum of photodegradation efficiency for MB was obtained at 0.1% of photocatalyst ZnO. On the other hand, when the addition of photocatalyst was used beyond optimum, the photodegradation efficiency began to decline with the further increasement of ZnO particles. This can be attributed to the reduction for the penetration of light through the solution that is usually caused by the increase in the turbidity of the solution. This is known as light screening effect (Pardeshi and Patil 2008). Moreover, in such condition, a part of the photocatalyst particles may agglomerate and precipitate, which

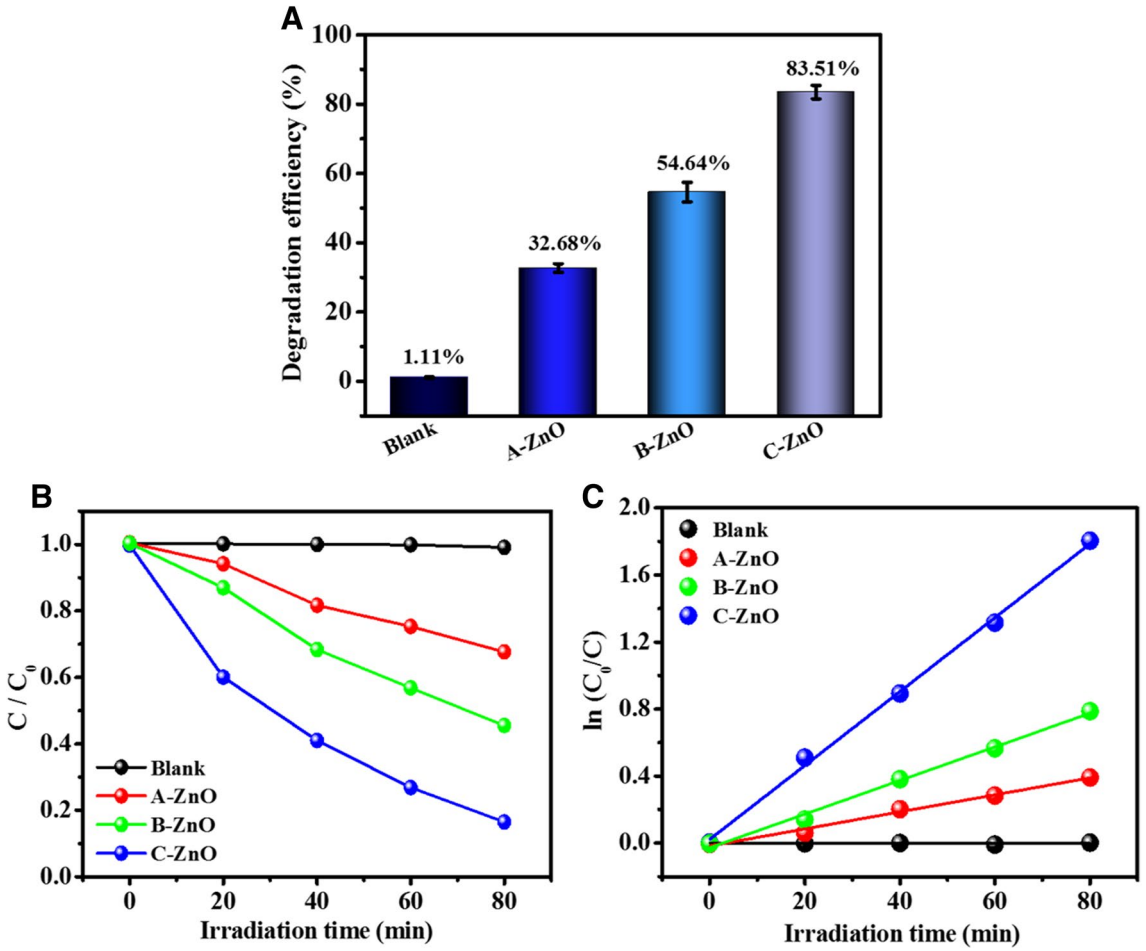

Fig. 7 Effects of ZnO catalysts with different morphologies on the photodegradation efficiency for MB aqueous solution under 250 W UV irradiation. **a** Photodegradation rates for three ZnO samples within 80 min. **b** Degradation profiles of MB as a function of irradiation time for different ZnO catalysts. **c** Photocatalytic degradation kinetic curves of MB solution catalyzed by distinct ZnO particles. The treatment in the absence of ZnO particles is served as blank control group

is thus unfavorable to the photodegradation (Konstantinou and Albanis 2004).

In addition, it has been reported that pH is a significant influential parameter for the degradation of organic substances (Lee et al. 2016). Thus, keeping other conditions in the photocatalytic reaction system unchanged, the effect of the initial pH value of the reaction system on the photodegradation efficiency of organic dye catalyzed by C-ZnO was evaluated in this study and the corresponding results are shown in Fig. 9. It is clear that the higher pH value in the above reaction system for C-ZnO contributes to its faster degradation under 250 W UV irradiation. When the pH value of the implemented solution was adjusted to be 10.5 by alkali liquor, the photocatalytic degradation efficiency of MB for leaf-like C-ZnO can reach 92.9%. And the color of MB solution changed from blue to colorless within less than 20 min (Fig. 9), indicating that the alkaline condition may be conducive to the photodegradation of organic pollutants for C-ZnO catalyst. This may be due to the fact that the change of pH can affect the charge distribution on the surface of nanoscale zinc oxide particles, which can further change the number and migration rate of photogenerated electron–hole pairs on the particle surface and ultimately affect the photocatalytic activity of ZnO (Abdollahi et al. 2011; Najam Khan and Dutta 2015). Meanwhile, for the control group without the addition of photocatalyst ZnO, the color of methylene blue solution hardly changed in a series of reaction time under different pH conditions (as depicted in Fig. 9).

Mechanism of morphology-dependent photodegradation

It is a known fact that the morphology of ZnO particles can be facilely modulated by regulating the reaction conditions. As conducted in this research, ZnO powder was made up of numerous aggregated nanosheets with leaf-like superstructure

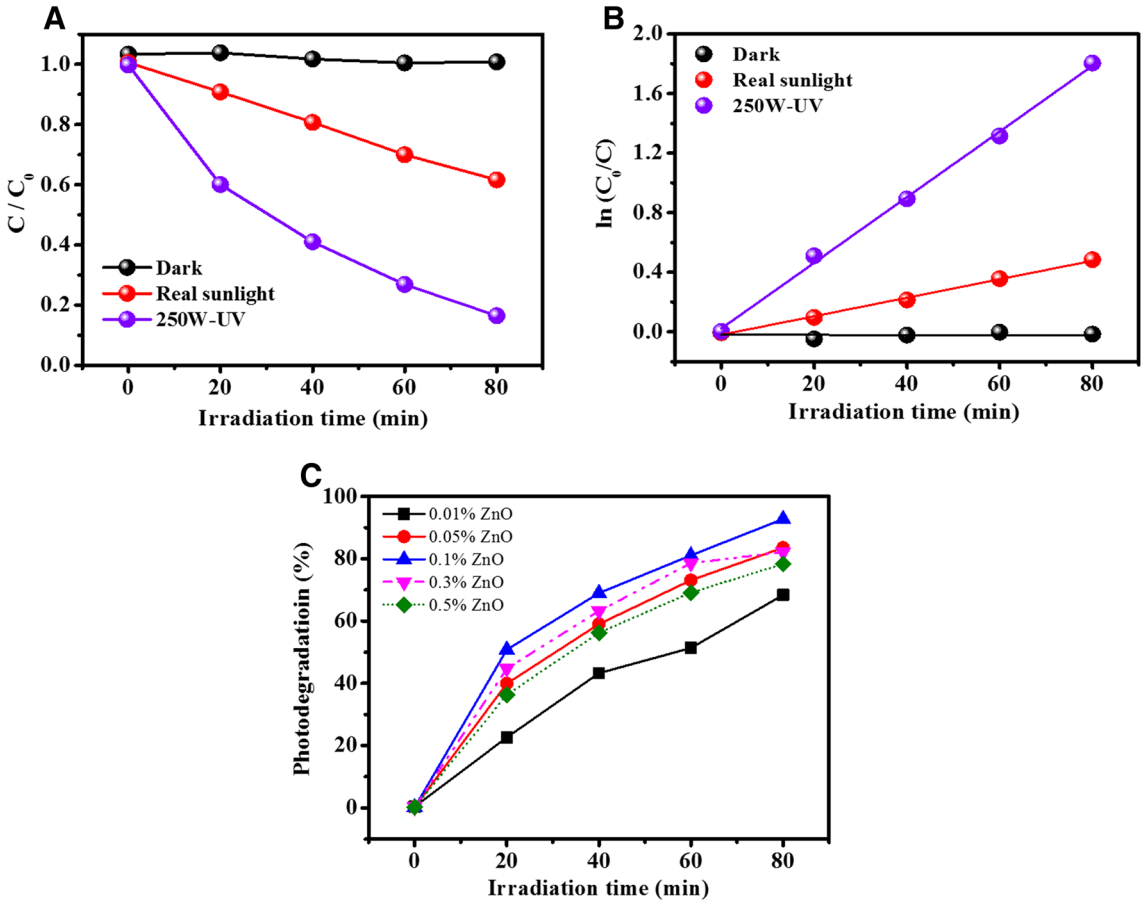

Fig. 8 Effects of illumination modes (**a** and **b**) and catalyst concentrations (**c**) on photodegradative efficiency for leaf-like C-ZnO, including degradation profiles of MB solution with reaction time (**a** and **c**) and photocatalytic degradation kinetic curves of MB solution under 250 W UV irradiation **b**

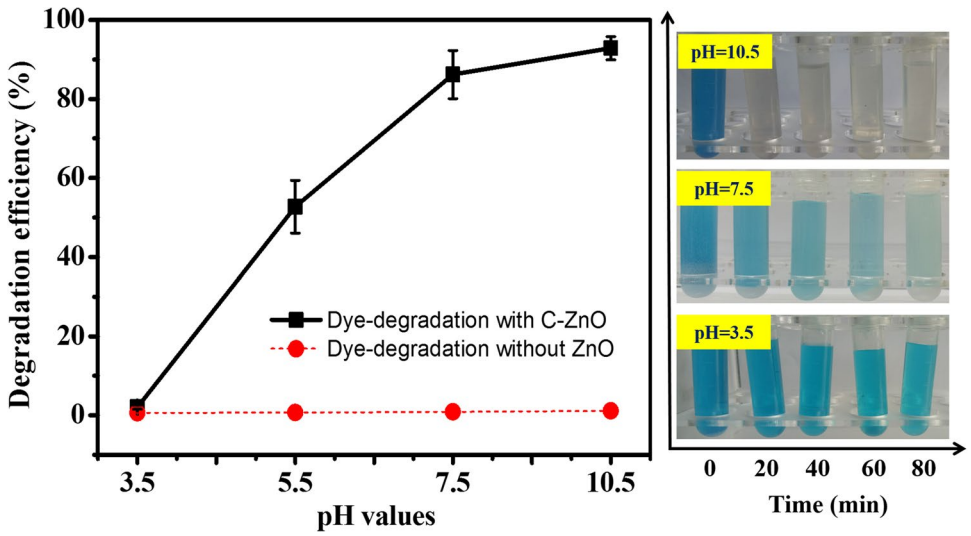

Fig. 9 Effects of different pH conditions on photodegradation percentage of MB solution for C-ZnO under 250 W UV irradiation

at a relatively low temperature (60 °C). When the reaction temperature rises to 90 °C, an individual flower-like branchy array composed of nanorods was formed. This is primarily related to the crystal growth characteristics of ZnO with wurtzite structure. As the reaction temperature rises, both the energy of the reactant and the number of active reaction molecules

increase, which in turn are beneficial to the formation of $Zn(OH)_4^{2-}$ growth unit and the final flower-shaped crystallites (Hui et al. 2016). With the addition of citric acid, the ZnO crystal growth along [001] polar direction is hindered due to negatively charged citrate ions are absorbed on the Zn^{2+} ions of the (001) surface (Mujtaba 2015; Nicholas et al. 2012). Meanwhile, growing units of $Zn(OH)_4^{2-}$ are prone to attach and dehydrate on the $(01\bar{1}0)$ planes and promote the growth perpendicular to the [001] orientation (Wang et al. 2017). However, the higher concentration of citrate ions, the stronger chelation between Zn^{2+} and citrate ions, and the nanosheets assembled more tightly. As a consequence, the crystalline morphology of ZnO transformed gradually to bumpy spheres. Therefore, distinct morphology and structure of ZnO crystals such as flower-like, leaf-like and sphere-like have changed exposed crystal planes. Since the photocatalytic capacity is mainly realized on the surface of metal oxides, the morphology and structure of ZnO crystal is bound to affect its photocatalytic performance. Illuminated by sufficient intensity of irradiation (the energy of photons ≥ the band gap energy), the conduction-band electrons and equal amount of valence-band holes are emerged on the surface of ZnO crystal as depicted in Eq. (1). And then the photo-generated holes can react with the associated H_2O or OH^- groups to breed reactive hydroxyl radicals (OH·) as in Eqs. (2) and (3). Meanwhile, electrons in the conduction band can react with oxygen by forming superoxide radicals ($O_2^{\cdot -}$) and further form more hydroxyl radicals (OH·) followed by Eqs. (4) and (5). Thereafter, the existence of these OH· radicals can further react with the MB molecules to mineralize these organic pollutants according to Eq. (6) (Wang et al. 2017). In fact, the energy band of ZnO crystal determines that it absorbs only ultraviolet light, while ultraviolet radiation in sunlight only accounts for 5%. That is why the photocatalytic performance driven by 250 W UV is better than that for real sunlight illumination. Based upon the above reaction mechanism, the alkaline environment contributes to the formation of free hydroxyl radicals, which in turn can speed up the photocatalytic efficiency. More importantly, a larger surface area can not only lead to more dye immobilization, but generate more photo-induced electrons and holes (Pung et al. 2012). Among the three different types of ZnO samples, C-ZnO crystal in this study was assembled by a number of leaf-like nanoarrays and possessed a superior surface area, thus providing it excellent photocatalytic activity.

$$ZnO + hv \rightarrow h^+ + e^- \quad (1)$$

$$h^+ + H_2O \rightarrow OH\cdot + H^+ \quad (2)$$

$$h^+ + OH^- \rightarrow OH\cdot \quad (3)$$

$$e^- + O_2 \rightarrow O_2^{\cdot -} \quad (4)$$

$$O_2^{\cdot -} + H^+ \rightarrow 2OH\cdot \quad (5)$$

$$OH\cdot + MB \rightarrow CO_2 + H_2O \quad (6)$$

Conclusions

In summary, ZnO particles with various morphologies were successfully synthesized via a facile one-step wet chemical approach. By reasonably altering reaction parameters, the produced ZnO samples were identified as flower-like, sphere-like and leaf-like crystalline superstructures, respectively. The catalytic study shows that the photodegradation of organic dye is largely related to the morphology and structure of catalyst. A possible regulation mechanism of morphology-dependent photodegradation by ZnO was proposed according to the experimental results. It was proved that leaf-like ZnO nanosheets have better performance for MB degradation as compare to rod and sphere nanoarrays due to its larger surface area which is beneficial to the adsorption of organic pollutant and the enhancement of optical quality. Moreover, this work indicates that photocatalytic efficiency can be further improved by creating favorable reaction conditions, such as radiation intensity and alkaline environment. This study could suggest the possibility to fabricate the morphology and catalytic efficiency of the prepared nanomaterial and extend its potential applications in photodegradation and other applied surface categories.

Acknowledgements The authors gratefully acknowledge the financial support of the Science and Technology Research Program of Chongqing Municipal Education Commission (Grant No. KJ 1758498) and Chongqing Normal University Foundation Program (Grant No. 17XL13006) and. Thanks also to the technical support from Institute for Clean Energy & Advanced Materials, Faculty of Materials & Energy in Southwest University.

References

Abdollahi Y, Abdullah AH, Zainal Z, Yusof NA (2011) Photocatalytic degradation of p-cresol by zinc oxide under UV irradiation. Int J Mol Sci 13(1):302–315

Ali I (2014) Water treatment by adsorption columns: evaluation at ground level. Sep Purif Rev 43(3):175–205

Ali A, Ambreen S, Javed R, Tabassum S, Haq IU, Zia M (2017) ZnO nanostructure fabrication in different solvents transforms physiochemical, biological and photodegradable properties. Mater Sci Eng C 74:137–145

Allegre C, Maisseu M, Charbit F, Moulin P (2004) Coagulation-flocculation-decantation of dye house effluents: concentrated effluents. J Hazard Mater 116(1–2):57–64

Anas S, Rahul S, Babitha KB, Mangalraja RV, Ananthakumar S (2015) Microwave accelerated synthesis of zinc oxide nanoplates and their enhanced photocatalytic activity under UV and solar illuminations. Appl Surf Sci 355:98–103

Arfaoui MA, Dolez PI, Dubé M, David É (2017) Development and characterization of a hydrophobic treatment for jute fibres based on zinc oxide nanoparticles and a fatty acid. Appl Surf Sci 397:19–29

Assadi A, Dehghani MH, Rastkari N, Nasseri S, Mahvi AH (2012) Photocatalytic reduction of hexavalent chromium in aqueous solutions with zinc oxide nanoparticles and hydrogen peroxide. Environ Prot Eng 38

Carraway ER, Hoffman AJ, Hoffmann MR (1994) Photocatalytic oxidation of organic acids on quantum-sized semiconductor colloids. Environ Sci Technol 28(5):786

Cho S, Jang JW, Jung SH, Bo RL, Oh E, Lee KH (2009) Precursor effects of citric acid and citrates on ZnO crystal formation. Langmuir the ACS J Surf Colloids 25(6):3825

Chuang CC, Prasannan A, Huang BR, Hong PD, Chiang MY (2017) Simple synthesis of eco-friendly multifunctional silk-sericin capped zinc oxide nanorods and their potential for fabrication of hydrogen sensors and UV photodetectors. ACS Sustain Chem Eng 5(5)

Das S, Samanta A, Jana S (2017) Light-assisted synthesis of hierarchical flower-like MnO_2 nanocomposites with solar light induced enhanced photocatalytic activity. ACS Sustain Chem Eng 5(10)

Du P, Song L, Xiong J, Cao H (2013) Photocatalytic degradation of Rhodamine B using electrospun TiO_2 and ZnO nanofibers: a comparative study. J Mater Sci 48(24):8386–8392

Fox MA, Dulay MT (1993) Heterogeneous photocatalysis. Chem Rev 93(1):341–357

Hegab HM, Zou L (2015) Graphene oxide-assisted membranes: fabrication and potential applications in desalination and water purification. J Membr Sci 484:95–106

Hernandez S, Hidalgo D, Sacco A, Chiodoni A, Lamberti A, Cauda VA, Tresso EM, Saracco G (2015) Comparison of photocatalytic and transport properties of TiO_2 and ZnO nanostructures for solar-driven water splitting. Phys Chem Chem Phys 17(12):7775–7786

Hong D, Zang W, Xiao G, Fu Y, He H, Jing S, Xing LL, Liu B, Xue X (2016) High piezo-photocatalytic efficiency of CuS/ZnO nanowires co-using solar and mechanical energy for degrading organic dye. ACS Appl Mater Interfaces 8(33):21302

Hui A, Liu J, Ma J (2016) Synthesis and morphology-dependent antimicrobial activity of cerium doped flower-shaped ZnO crystallites under visible light irradiation. Colloids Surf A Physicochem Eng Asp 506:519–525

Konstantinou IK, Albanis TA (2004) TiO_2-assisted photocatalytic degradation of azo dyes in aqueous solution: kinetic and mechanistic investigations: a review. Appl Catal B 49(1):1–14

Lee KM, Lai CW, Ngai KS, Juan JC (2016) Recent developments of zinc oxide based photocatalyst in water treatment technology: a review. Water Res 88:428–448

Li Y, Xie W, Hu X, Shen G, Zhou X, Xiang Y, Zhao X, Fang P (2010) Comparison of dye photodegradation and its coupling with light-to-electricity conversion over TiO and ZnO. Langmuir 26(1):591–597

Miao Y, Zhang H, Yuan S, Jiao Z, Zhu X (2016) Preparation of flower-like ZnO architectures assembled with nanosheets for enhanced photocatalytic activity. J Colloid Interface Sci 462:9–18

Mujtaba J (2015) Fine control over the morphology and photocatalytic activity of 3D ZnO hierarchical nanostructures: capping vs. etching. RSC Adv 5(69):56232–56238

Mujtaba J, Sun H, Fang F, Ahmad M, Zhu J (2015) Fine control over the morphology and photocatalytic activity of 3D ZnO hierarchical nanostructures: capping vs. etching. RSC Adv 5(69):56232–56238

Najam Khan M, Dutta J (2015) Comparison of photocatalytic activity of zinc stannate particles and zinc stannate/zinc oxide composites for the removal of phenol from water, and a study on the effect of pH on photocatalytic efficiency. Mater Sci Semicond Process 36:124–133

Nguyen T, Roddick FA, Fan L (2012) Biofouling of water treatment membranes: a review of the underlying causes, monitoring techniques and control measures. Membranes 2(4):804

Nicholas NJ, Franks GV, Ducker WA (2012) Selective adsorption to particular crystal faces of ZnO. Langmuir 28(18):7189–7196

Pardeshi SK, Patil AB (2008) A simple route for photocatalytic degradation of phenol in aqueous zinc oxide suspension using solar energy. Sol Energy 82(8):700–705

Pung SY, Lee WP, Aziz A (2012) Kinetic study of organic dye degradation using ZnO particles with different morphologies as a photocatalyst. Int J Inorg Chem 2012 (2)

Ratna B (2012) Pollution due to synthetic dyes toxicity & carcinogenicity studies and remediation. Int J Environ Sci 3(3):940

Sonderegger T, Pfister S, Hellweg S (2015) Criticality of water: aligning water and mineral resources assessment. Environ Sci Technol 49(20):12315–12323

Wang Y, Zhu S, Chen X, Tang Y, Jiang Y, Peng Z, Wang H (2014) One-step template-free fabrication of mesoporous ZnO/TiO_2 hollow microspheres with enhanced photocatalytic activity. Appl Surf Sci 307(18):263–271

Wang C, Gao Y, Wang L, Li P (2017) Morphology regulation, structural, and photocatalytic properties of ZnO hierarchical microstructures synthesized by a simple hydrothermal method. Physica Status Solidi 214(6):1600876

Xue X, Zang W, Deng P, Wang Q, Xing L, Zhang Y, Wang ZL (2015) Piezo-potential enhanced photocatalytic degradation of organic dye using ZnO nanowires. Nano Energy 13:414–422

Zhao R, Wang Y, Li X, Sun B, Wang C (2015) Synthesis of β-cyclodextrin-based electrospun nanofiber membranes for highly efficient adsorption and separation of methylene blue. Acs Appl Mater Interfaces 7(48):26649–26657